

1 Introduction

Molecular hydrogen (H_2) is the second most abundant reduced compound in the atmosphere after methane (CH_4). H_2 is not a radiatively active gas itself, but – via its role in atmospheric chemistry – it indirectly influences the lifetime of the greenhouse gas CH_4 and several air pollutants (Prather, 2003; Schultz et al., 2003; Tromp et al., 2003; Warwick et al., 2004; Jacobson, 2008; Feck et al., 2008; Ehhalt and Rohrer, 2009; Popa et al., 2015). The main H_2 sources are photo-oxidation of CH_4 and non-methane volatile organic compounds (NMVOC) in the atmosphere and combustion processes at the surface, whereas soil deposition and oxidation by hydroxyl radicals (HO^*) are the main sinks. Oceans are a minor but significant source to the global H_2 budget with a mean estimated contribution of 7%. However, estimates of the oceanic contribution range from 1 to 15% in different studies, indicating high uncertainties (Novelli et al., 1999; Hauglustaine and Ehhalt, 2002; Ehhalt and Rohrer, 2009, and references herein; Pieterse et al., 2013).

Oceanic H_2 production is assumed to be mainly biological, as a by-product of nitrogen (N_2) fixation (e.g. Conrad, 1988; Conrad and Seiler, 1988; Moore et al., 2009, 2014). H_2 is produced during N_2 fixation in equimolar proportions, but also reused as an energy source. The H_2 net production rate during N_2 fixation depends on environmental conditions and also on microbial species (Bothe et al., 1980, 2010; Tamagnini et al., 2007; Wilson et al., 2010a). Besides N_2 fixation, abiotic photochemical production from chromophoric dissolved organic matter (CDOM) and small organic compounds such as acetaldehyde or syringic acid has also been found to be a source of hydrogen in the oceans (Punshon and Moore, 2008a, and references therein).

Unfortunately, measurements that constrain the temporal and spatial patterns of oceanic H_2 emissions to the atmosphere are sparse. Vertical profiles display highest concentrations in the surface layer (up to 3 nmol L^{-1}) and a sharp decrease with depth towards undersaturation, where the reasons for the undersaturation are not fully understood yet (e.g. Herr et al., 1981; Scranton et al., 1982; Conrad and Seiler, 1988).

16433

Tropical and subtropical surface waters are supersaturated up to 10 times or even more with respect to atmospheric H_2 equilibrium concentrations, and therefore a source of H_2 to the atmosphere. This is in contrast to temperate and polar surface waters, which are generally undersaturated in H_2 (Scranton et al., 1982; Herr et al., 1981, 1984; Herr, 1984; Conrad and Seiler, 1988; Seiler and Schmidt, 1974; Lilley et al., 1982; Punshon et al., 2007; Moore et al., 2014).

Additional information to constrain the global H_2 budget and to gain insight into production pathways comes from the analysis of the H_2 isotopic composition (quantitatively expressed as isotope delta value, δD , see Sect. 2.2). Different sources produce H_2 with characteristic δD values. Moreover, the kinetic isotope fractionation in the two main removal processes, soil deposition and reaction with HO^* , is different. The combined action of sources and sinks leads to tropospheric H_2 with a δD of +130‰ relative to Vienna Standard Mean Ocean water (VSMOW), (Gerst and Quay, 2001; Rhee et al., 2006; Rice et al., 2010; Batenburg et al., 2011). In sharp contrast, surface emissions of H_2 from fossil fuel combustion and biomass burning have δD values of approximately –200 and –300‰, respectively (Gerst and Quay, 2001; Rahn et al., 2002; Röckmann et al., 2010a; Vollmer et al., 2010). As originally proposed by Gerst and Quay (2001), isotopic budget calculations require the photochemical sources of H_2 to be enriched in deuterium, with δD values between +100 and +200‰ (Rahn et al., 2003; Röckmann et al., 2003, 2010b; Feilberg et al., 2007; Nilsson et al., 2007, 2010; Pieterse et al., 2009). Biologically produced H_2 has the most exceptional isotopic composition with δD of approximately –700‰ (Walter et al., 2012), reflecting strong preference of biogenic sources for the lighter isotope 1H .

The aim of the study was (i) to determine the δD of dissolved H_2 and gain more information about possible sources, and (ii) to get a high-resolution picture of the distribution of atmospheric H_2 along meridional Atlantic transects during different seasons and compare it with global model results. Samples were taken on four cruises along meridional Atlantic transects in the southern and Northern Hemisphere and on one

16434

cruise at the coast of Mauretania. A total of almost 400 atmospheric and 22 ocean surface water samples were taken, covering two seasons between 2008 and 2010.

2 Methods

2.1 Cruise tracks

5 During four cruises of RV *Polarstern* and one of RV *L'Atalante* between February 2008 and May 2010, air and seawater samples were collected (see Fig. 1, Table 1). The cruises of RV *Polarstern* were part of the OCEANET project (Autonomous measuring platforms for the regulation of substances and energy exchange between ocean and atmosphere, Hanschmann et al., 2012).

10 They covered both hemispheres, between Punta Arenas (Chile, 53° S / 71° W) and Bremerhaven (Germany, 53° N / 8° E). South–north transects were carried out in boreal spring (April/May) and north–south transects in boreal autumn (October/November). The transects followed similar tracks as the Atlantic Meridional Transect (AMT) programme (<http://amt-uk.org/>) and crossed a wide range of ecosystems and oceanic regimes, from sub–polar to tropical and from euphotic shelf seas and upwelling systems to oligotrophic mid–ocean gyres (Robinson et al., 2009; Longhurst, 1998).

15 The RV *L'Atalante* followed a cruise track from Dakar (Senegal) to Mindelo (Cape Verde), covering a sampling area along the coast of Mauritania and a transect to the Cape Verde Islands. This area is characterized by strongly differing hydrographical and biological properties with an intensive seasonal upwelling. Area and cruise track are described in more detail in Walter et al. (2013) and Kock et al. (2008).

2.2 Atmospheric air sampling

20 Discrete atmospheric air samples were taken on-board RV *Polarstern* at the bridge deck, using 1 L borosilicate glass flasks coated with black shrink-hose (NORMAG), with 2 Kel-F (PCTFE) O-ring sealed valves. The flasks were pre-conditioned by flushing with
16435

N_2 at 50 °C for at least 12 h; the N_2 remained in the flask at ambient pressure until the sampling. During sampling the flasks were flushed for 4 min with ambient air at a flow rate of 12 L min⁻¹ using Teflon tubes and a membrane pump (KNF VERDER PM22874-86 N86ANDC). The sample air was dried with Drierite[®] ($CaSO_4$). The flasks were finally
5 pressurized to approximately 1.7 bar, which allows duplicate measurements of the H_2 isotopic composition of an air sample.

Table 1 gives an overview of the sampling scheme for discrete H_2 samples. In total 360 samples were collected, regularly distributed over the transects at 4 to 6 h intervals. In 2009 the resolution of sampling was enhanced to one sample per two hours and
10 focused on five sub-sections of the transect, in an attempt to resolve dial variability.

Samples were always taken at the downwind side of the ship to exclude a possible contamination by ship diesel exhaust. One atmospheric sample was taken directly inside the ship's funnel of RV *Polarstern* to determine the mole fraction and δD of ship diesel exhaust as a possible contamination source. This first measurements for
15 ship diesel exhaust gave an H_2 mole fraction of (930.6 ± 3.2) nmol mol⁻¹ and a δD of (-228.6 ± 5.0) ‰. In the following, we will use the abbreviation “ppb” = 10⁻⁹ in place of the SI unit “nmol mol⁻¹”.

2.3 Headspace sampling from surface waters

In addition to the atmospheric air samples, 16 headspace samples from surface water were taken during the RV *Polarstern* cruise ANT-XXVI/4 in April/May 2010 and 6 samples during the RV *L'Atalante* cruise in February 2008. The experimental setup (Fig. 2) was a prototype, and deployed for the first time to extract headspace air from surface water for isotopic composition measurements of molecular H_2 . It consists of a glass vessel (10 L) and an evacuation/headspace sampling unit.

25 The glass vessel was evacuated for at least 24 h before sampling, using a Pfeiffer vacuum DUO 2.5A pump, with a capacity of 40 L min⁻¹ (STP: 20 °C and 1 bar). Water samples were taken from 5 m depth (RV *Polarstern* cruises) or 10 m depth (RV

L'Atalante cruise) using a 24-Niskin-bottle rosette with a volume of 12 L each. Sampling started immediately after return of the bottle rosette on-board and from a bottle dedicated to the H₂ measurements. The evacuated glass vessel was connected to the Niskin bottle by Teflon tubing, which was first rinsed with approximately 1 L surface water. Then, 8.4 L water streamed into the evacuated flask (Fig. 2), using a drip to enhance the dispersion of the sample water. After connection of the headspace-sampling unit, the lines were first evacuated and then flushed with a makeup gas several times. During the RV *L'Atalante* cruise a synthetic air mixture with an H₂ mixing ratio below threshold was used as makeup gas. The makeup gas used during the RV *Polarstern* cruises was a synthetic air mixture with an H₂ mole fraction of (543.9 ± 0.3) ppb and a δD of (93.1 ± 0.2) ‰. The mole fraction of the makeup gas was determined by the Max Planck Institute for Biogeochemistry and is given on the MPI2009 scale (Jordan and Steinberg, 2011). The glass vessel was pressurized to approximately 1.7 bar absolute with the makeup gas and the total headspace (added makeup gas plus extracted gas from the water sample) was then flushed to a pre-evacuated sample flask. The flasks were of the same type as for the atmospheric sampling: 1 L borosilicate glass flasks (NORMAG), coated with black shrink-hose to minimize photochemical reactions inside and sealed with 2 Kel-F (PCTFE) O-ring sealed valves. All flasks were previously conditioned by flushing with N₂ at 50 °C for at least 12 h and evacuated for at least 12 h directly before use.

The whole sampling procedure took around 15 min: (4.0 ± 0.5) min flushing surface water to the evacuated glass vessel, (8.0 ± 1.0) min to connect the glass vessel to the sampling unit and evacuate the lines, and (3.0 ± 0.5) min to add and pressurize the glass vessel with the makeup gas and take the headspace sample. The surface water temperature was on average (0.9 ± 0.6) °C higher than the air temperature. Given that most of the apparatus was at air temperature and that the headspace will adjust to ambient temperature relatively quickly during equilibration the air temperature was used for calculations. Since the temperature dependence of H₂ solubility is less than 0.3 % K⁻¹ for seawater between 16 and 30 °C (as encountered here) and view of the

16437

large H₂ supersaturations (see below), the error associated with this assumption is negligible. Flasks were stored in the dark until measurement. At the same location of headspace sampling also atmospheric samples were taken (Table 4).

2.4 Measurements

2.4.1 Atmospheric H₂ and δD (H₂) in discrete samples

The mole fraction and isotopic composition of molecular H₂ was determined using the experimental setup developed by Rhee et al. (2004) and described in detail in Walter et al. (2012, 2013) and Batenburg et al. (2011). The D/¹H molar ratio in a sample, R_{sample} (D/H), is quantified as the relative deviation from the D/¹H molar ratio in a standard, R_{standard} (D/H), as isotope delta δD value, and reported in per mill (‰):

$$\delta\text{D} = \frac{R_{\text{sample}}(\text{D}/\text{H})}{R_{\text{standard}}(\text{D}/\text{H})} - 1 \quad (1)$$

The isotopic standard is Vienna Standard Mean Ocean Water (VSMOW). H₂ mole fractions are reported as mole fractions in nmol mol⁻¹, abbreviated ppb (10⁻⁹, parts per billion) and linked to the MPI2009 calibration scale for atmospheric hydrogen (Jordan and Steinberg, 2011). As working standards, atmospheric air from laboratory reference air cylinders and synthetic air mixtures were used (Walter et al., 2012, 2013; Batenburg et al., 2011); the H₂ mole fractions of the air in these cylinders were determined by the Max Planck Institute for Biogeochemistry, Jena, Germany. The atmospheric reference air and the synthetic isotope reference air were measured daily (atmospheric reference air at least twice) and results were used for correction of the sample measurements. The uncertainties reported here reflect random (i.e. repeatability) errors only and do not include possible systematic errors (Batenburg et al., 2011; Walter et al., 2012, 2013). Samples were measured in random order and analysed within 3 months (ANT-XXIV/4, ANT-XXV/5, ANT-XXVI/1) up to two years (ANT-XXVI/4) after sampling. Storage tests

16438

indicate that glass flasks equipped with Kel-F valves are stable for H₂ (Jordan and Steinberg, 2011). The mean measurement repeatability between the two measurements on the same flask was between ±3.2 ppb (ANT-XXV/5, *n* = 14) and ±6.4 ppb (ANT-XXVI/4, *n* = 108) for the mole fraction and ±3.4‰ (ANT-XXVI/4, *n* = 108) and ±5.0‰ (ANT-XXV/5, *n* = 14) for the isotopic composition.

H₂ and CO mole fractions were also measured by using a Peak Performer 1 RGA with synthetic air as a carrier gas, either continuously on-board (ANT-XXVI/4, see Sect. 2.4.2) or from discrete flasks in the laboratory (ANT-XXV/5 and ANT-XXVI/1). The discrete RGA measurements were performed from the same glass flasks after measurement of the isotope system (see above). Due to a remaining slight overpressure in the flasks, an active pumping of the air into the RGA was not necessary and the flasks were simply connected to the RGA inlet by Teflon tubing. The remaining pressure was mostly sufficient to perform 8 to 10 measurements. A slight memory effect was observed and thus only the last 5 measurements were taken into account when stable. Samples with only three or less valid measurements were not used for evaluation. The standards were the same as those used for the isotope system. For both cruises (ANT-XXV/5 and ANT-XXVI/1), the mean measurement repeatability was better than ±0.8% (H₂) and ±2% (CO). A comparison between the H₂ mole fractions measured with the Peak Performer 1 RGA and the isotopic experimental setup reveals on average slightly lower RGA values of (7.5 ± 23.8) ppb (see Fig. 3).

2.4.2 Atmospheric H₂ measured continuously

For the on-board continuous measurements of H₂ mole fractions a Peak Performer 1 RGA was used. The atmospheric air was drawn from the bridge deck to the laboratory in 1/4 inch Decabon tubing. The CO mole fraction was also measured in the same measurement and will be reported here for information, but without further discussion.

In alternating order, 10 air samples and 10 aliquots of reference air were measured, using synthetic air as carrier gas. Due to small memory effects, only the last 5 measurements of each were taken into account when the values were stable. The mole

16439

fractions of H₂ and CO were calculated by using the mean of the enclosing standard measurements, with an estimated maximal error of ±5%. For more details see Popa et al. (2014). The mean measurement repeatability for the air samples was ±1.7% for H₂ and ±3.6% for CO in ambient air, respectively ±0.8% (H₂) and ±0.9% (CO) for the reference air. Comparing the H₂ mole fractions measured continuously on the RGA with discrete samples measured on the isotope system and collected close in time, we found a mean offset of (-18.8 ± 16.4) ppb for the RGA results.

2.4.3 Dissolved H₂ extracted from surface water

The discrete samples of extracted dissolved H₂ were measured as described for the discrete atmospheric samples in Sect. 2.4.1. Details about assumptions and calculations to determine dissolved H₂ concentrations and isotope delta values and quantity symbols are given in detail in the Supplement.

Defining the extraction efficiency η as

$$\eta = \frac{c_h V_h}{c_{w0} V_w} \quad (2)$$

where V_h and V_w are the volume of the headspace and the water fraction, and c_h the concentration of H₂ in the headspace. The initial concentration of H₂ in seawater, c_{w0} , can be calculated from

$$c_{w0} = \frac{c_h V_h}{\eta V_w} \quad (3)$$

The concentration in the headspace, c_h , was not measured directly, but can be derived from the measured H₂ mole fraction in the sampling flask. The sampling procedure following gas extraction under vacuum can be broken into three steps (see Methods section):

1. Expansion of the headspace into the gas transfer system

16440

2012) model of the National Oceanic and Atmospheric Administration (NOAA, <http://ready.arl.noaa.gov/HYSPLIT.php>).

2.5 Modeling

2.5.1 TM5 model

5 We performed simulations of H_2 mole fractions and isotopic composition with the global chemistry transport model TM5 (Krol et al., 2005), and compared them with our measurement data (Fig. 5). The simulation setup was similar to the one of Pieterse et al. (2013) and only a short description is given here. The model version used employs the full hydrogen isotopic scheme from Pieterse et al. (2009) and uses ERA-
10 Interim meteorological data. The chemistry scheme is based on CBM-4 (Houweling et al., 1998), which has been extended to include the hydrogen isotopic scheme (that is, for all chemical species that include hydrogen atoms, HH and HD are treated separately and have different reaction rates). The H_2 sources and isotopic signatures are given as input; these and also the H_2 soil deposition velocities are identical to Pieterse et al. (2013).
15

The model has a relatively coarse spatial resolution of 6° longitude by 4° latitude, and a time step of 45 min. Daily average mole fraction fields are used for comparison to observations. The model results were interpolated to the time and location of the observations.

2.5.2 Global oceanic emissions

20 The climatological global oceanic emissions were calculated using the protocol of Pieterse et al. (2013), based on the GEMS database and an assumed mean oceanic H_2 source of 5 Tg a^{-1} as given from global budget calculations (see Ehhalt and Rohrer, 2009, and references therein, Pieterse et al., 2013). The spatial and temporal variability

16443

of oceanic H_2 emissions caused by N_2 fixation are adopted from the spatial and temporal distribution of oceanic CO (Erickson and Taylor, 1992).

3 Results and discussion

3.1 Atmospheric H_2 transects

5 Our data set includes data of two hemispheres and two seasons between 2008 and 2010 (see Table 2, Fig. 4). The mean mole fraction of H_2 ranged between (532.0 ± 10.7) ppb and (548.5 ± 6.8) ppb. In spring, the mean values were almost equal between the hemispheres with approximately 1 to 2 ppb difference, but they differed significantly in autumn. In this season, the mean values in the Northern Hemisphere (NH) were
10 approximately 16 ppb or 3% lower compared to the Southern Hemisphere (SH), with a distinct transition between the hemispheres at around 8° N. In contrast, δD differed significantly between the hemispheres in both seasons. In the Southern Hemisphere, absolute δD values were always between 9 and 27‰ higher than in the Northern Hemisphere, and generally remained within a narrow range between (140.5 ± 21.1) ‰
15 and (145.4 ± 5.3) ‰. In contrast to the mole fraction, isotope delta differences between the hemispheres were less pronounced in autumn than in spring. These two seasonal patterns, in the following defined as “summer signal” and “winter signal”, are mainly caused by biological processes and tropospheric photochemistry and driven by variations in the NH. They are in line with previously published data and model results (Rhee et al., 2006; Price et al., 2007; Rice et al., 2010; Pieterse et al., 2011, 2013; Batenburg et al., 2011; Yver et al., 2011; Yashiro et al., 2011).
20

The “summer signal”, observed in October, is characterized by lower H_2 mole fractions in the Northern Hemisphere and a less pronounced difference in δD between the hemispheres. Deposition by biological activity of microorganisms in the soils is the main
25 sink of H_2 (Yonemura et al., 2000; Pieterse et al., 2013) and the sink strength in the northern and Southern Hemisphere depends on the distribution of landmasses and on

16444

season. With approximately 70 % of landmasses in the NH and higher microbial activity in the summer, the mole fraction during this season is lower in the NH than in the SH. Due to the general preference of organisms for molecules with lighter isotopic composition, the δD values increase during summer in the NH and the interhemispheric gradient becomes less pronounced.

The “winter signal” observed in April is defined by almost equal mole fractions and more pronounced differences in δD values between the hemispheres. In winter, molecular hydrogen is accumulating in the NH hemisphere, and the main source is fossil fuel combustion with a depleted isotopic composition of -170 to -270 ‰ (Gerst and Quay, 2001; Rahn et al., 2002). This leads to nearly equal mole fractions in both hemispheres and a more pronounced δD gradient, with isotopically lighter H_2 in the NH. The contribution of source and sink processes in the SH to the seasonal patterns is less pronounced than for the NH (Pieterse et al., 2011, 2013). As a result, the H_2 seasonal cycle in the SH is much weaker compared to the NH. The SH isotopic H_2 signature is caused by mainly emissions and chemical loss with an isotope delta of approximately $+190$ ‰, which explains the generally higher δD values. The Intertropical Convergence Zone (ITCZ) separates the two hemispheres and is clearly visible, not only in the H_2 distribution, but also in the CO distribution.

Simulations of H_2 mole fractions and isotopic composition using the global chemistry transport model TM5 (Krol et al., 2005) compared with our atmospheric data reveal that the model simulates the H_2 mole fractions quite well (Fig. 5), with a slight overestimate of up to 20 ppb (which means up to 4 %).

The model results are less variable on small spatial scales, due to the low spatial resolution, and possibly to local influences that are not included in the model (e.g. ocean emissions in the model are less variable in time and space than they could be in reality). The largest differences between the modeled and measured H_2 occur between 30° S and the equator. This seems a systematic feature and could be due to a slight overestimation of sources or underestimation of sinks by the model. Despite these small differences, the model is consistent with measured H_2 mole fractions and

16445

simulates them well. Large-scale features are clearly visible, like the sharp gradient around 10° N during cruise ANT-XXVI/1 (Fig. 5, top, third plot), or the decrease in δD towards northern mid-latitudes (most evident for the cruises ANT-XXIV/4 and ANT-XXVI/4, first and last plots in Fig. 5, top). A slight overestimate of the H_2 mole fractions was also noted by Pieterse et al. (2013). This might be explained by an overestimate of photochemical sources in the model, which would influence only the mole fractions but not the δD values.

The model simulates the isotopic composition of H_2 even better than the mole fractions. The most important features are the general decrease from south to north, and the sharp gradient around the equator. As most sources and sinks of H_2 have very different isotopic signatures, this good comparison indicates that the model represents well both the magnitude and the isotopic signature of the main components of the H_2 cycle. Similar to Pieterse et al. (2013) we also observe a slight underestimate of the δD at high southern latitudes, which is possibly due to underestimating the isotopic composition assumed for H_2 returning from the stratosphere in the latitude band 60° S to 90° S.

3.2 Spatial and temporal high-resolution transects during ANT-XXV/5

In April 2009 the sampling resolution was increased to approximately one sample per two hours for five selected sections of the transect during ANT-XXV/5 (Fig. 4, Table 3): three in the Southern Hemisphere, one crossing the equator and one in the Northern Hemisphere. These transects were chosen based on previously published data (Herr et al., 1984; Conrad and Seiler, 1988) and with the aim to get an indication of small-scale sources or diurnal cycles of atmospheric H_2 for further investigations.

All transects showed neither a diurnal cycle nor a correlation with radiation and a range of δD values within or only slightly outside a 2σ range around the mean, except for the one between 23.5 to 15.7° S (Fig. 6a). Here the highest H_2 mole fractions of (631.9 ± 3.2) ppb, combined with the lowest δD values of (20.9 ± 5.0) ‰, were found around 16° S. Due to the limited spatial resolution and therefore low number of

16446

data points a Keeling plot analysis (Fig. 6b) of the data between 15 and 18° S was made with either 5, 7, or 9 data points to get a reasonable range for the source signature. It reveals a mean source signature of -561.5 in a range of -530 to -683 ‰ ($n = 7 \pm 2$, $R^2 = 0.85 \pm 0.01$). The correlation coefficient is a mean of the three analyses.

5 HYSPLIT trajectories for the samples collected on this transect during the 28 April and 1 May 2010 (21.8 to 15.7° S) reveal the same origin of air masses coming from the direction of Antarctica. Oceanographic parameters such as water temperature and salinity are similar and do not correlate with H₂ mole fractions and δD values. These findings indicate a strong but local source, and the low δD value for the source obtained
10 by the Keeling plot analysis points to biological production (Walter et al., 2012). Such local and temporal patchiness of high H₂ mole fractions in surface waters was reported previously in correlation to high N₂ fixation rates (Moore et al., 2009, 2014). Although reported for other oceanic regions the H₂ mole fractions and δD values here do neither show a diurnal cycle (Herr et al., 1984) nor they are correlated with radiation indicating
15 photochemical production (Walter et al., 2013), and most of the values were observed during night. Wilson et al. (2013) recently showed that H₂ production and uptake rates clearly depends on microbial species, and also on their individual day–night rhythm, but the contribution of different diazotrophs to the marine H₂ cycle is unknown (e.g. Bothe et al., 2010; Schütz et al., 2004; Wilson et al., 2010a, 2010b; Punshon and Moore, 2008b; Scranton, 1983; Moore et al., 2009).

20 Around 21.2° S one single sample with a low mole fraction of (393.9 ± 3.2) ppb in combination with a high δD of (322.45 ± 5) ‰ value was observed. As mentioned before HYSPLIT models reveal the same origin of air masses on this transect, thus this sample indicates probably a local sink. However, this interpretation depends on only
25 one single measurement point and although neither instrumental parameters indicated an outlier nor meteorological or oceanographical parameters differed from other samples, we cannot exclude an artefact due to sampling, storage, or analyses. A simple Rayleigh fractionation model reveals a fractionation factor of $\alpha = 0.646 \pm 0.002$, which is close to the value of oxidation by HO* ($\alpha = 0.58 \pm 0.07$, Batenburg et al., 2011). An

16447

estimate of the δD value by using an HO* oxidation fractionation factor would lead to an increase by 125 or 149‰, respectively. The observed increase of δD seems reasonable when assuming oxidation by HO*, but with respect to the HO* mole fraction and the slow reaction rate of H₂ + HO* it is questionable whether the H₂ decrease here
5 can be explained by this.

3.3 Dissolved H₂

3.3.1 H₂ concentration

In total 16 headspace samples were taken during the RV *Polarstern* cruise in April/May 2010 along the transect 32.53° W / 18.79° S to 13.00° W / 36.54° N and 6 samples during the RV *L'Atalante* cruise in February 2008 between 23.00–17.93° W
10 to 16.9–19.2° N to analyse the H₂ mole fraction and the isotopic composition (see Table 4).

15 Although our setup was a prototype with possibilities for improvement e.g. by adding a heat control or improved pressure monitoring, the mole fractions are in line with previously published data. The H₂ excess, $\Delta(H_2)$, exceeds 5 nmolL⁻¹, the saturation differ from close to equilibrium to 15-fold supersaturation. Highest supersaturation was found in the Southern Hemisphere between 16 and 11° S and in the Northern Hemisphere around the Cape Verde islands and the coast of Mauretania (Fig. 7a, Table 4).

18 Herr et al. (1984) reported patchy enhanced H₂ concentrations in the surface water with up to 5-fold supersaturation in the subtropical south Atlantic (18–31° W and 29–42° W). This is comparable to what Conrad and Seiler (1988) found in the Southern Atlantic, on a similar cruise track as the RV *Polarstern*. Around the equator they measured H₂ surface water concentrations up to 12-fold supersaturation. In the Southern Pacific, Moore et al. (2009) combined H₂ surface water measurements with N₂
20 fixation measurements. They reported a strong correlation between these parameters, a patchy distribution and a steep maximum of H₂ concentrations up to 12.6 nmolL⁻¹ around 14° S.
25

16448

The recently published data by Moore et al. (2014) show similar patterns across the Atlantic as we found, with highest values around the southern and northern subtropics. However, our saturations are lower than the ones given by them, especially in the Northern Hemisphere. Such differences might be caused by experimental issues such as overestimated extraction efficiency or can be due to real temporal variability as the sampling seasons differed. The extraction efficiency has been estimated as 92 % (see Supplement) and was incorporated into the calculation of the original seawater concentration. With respect to the assumption of biological production as main production pathway it is more likely that due to the different sampling seasons less H₂ was produced in April than in October/November because of less microbial activity especially on the Northern Hemisphere in boreal winter.

3.3.2 Isotopic composition of H₂

Additional information about H₂ sources comes from the analysis of the H₂ isotopic composition. In the literature only one experimental value of dissolved marine δD exists, $\delta D = -628\text{‰}$ (Price et al., 2007; Rice et al., 2010), but the origin of this value is unclear and it is based on unpublished data. Nevertheless, this value has been used as representative for oceanic emission in several global budget calculations (e.g. Price et al., 2007; Pieterse et al., 2011). Other authors (e.g. Rahn et al., 2003; Rhee et al., 2006) used a theoretical value of -700‰ , as expected for thermodynamic isotope equilibrium between H₂ and H₂O based on the calculations of Bottinga (1969). The results presented here are the first well-documented experimental results for isotope analysis of dissolved H₂ in seawater.

From the measurement of the isotopic composition of H₂ in the headspace we calculate the isotopic composition of H₂ that was originally dissolved in the sea water as described in Sect. 2.4.3 and in the Supplement, using two different assumptions for fractionation between dissolved H₂ and H₂ in the gas phase. The results shown in Table 4 reveal δD values for the dissolved H₂ that vary within a wide range of -112 to -719‰ for both fractionation scenarios. Interestingly, δD shows two distinct groups of

16449

samples that can be separated by the water temperature (Fig. 7b). In water masses with a temperature above 21 °C the δD values are $(-629 \pm 54)\text{‰}$ ($n = 14$), in water masses with a temperature of 20 °C or below δD values are $(-249 \pm 88)\text{‰}$ ($n = 8$). There is no correlation of δD with salinity (Fig. 7c), but the high temperature (and low δD) waters have also a generally higher supersaturation than the low temperature (high δD) waters (Fig. 7d).

The very depleted isotope signature of the H₂ in the warmer water masses is consistent with the values expected for biological production. The slight enrichment compared to the value of $\approx -700\text{‰}$ that is expected for biologically produced H₂ in equilibrium with ocean water (Bottinga, 1969; Walter et al., 2012) may be caused by a partial consumption within the water, which would enrich the remaining fraction. The relatively smooth distribution of the isotopic composition of H₂ in the atmosphere strongly indicates that the contribution from atmospheric variability cannot be a main contributor of the isotope variations observed in dissolved H₂, even within the group of the depleted samples.

To our knowledge this is the first time that oceanic production of H₂ has been directly attributed to biological processes by using isotope techniques. For the samples collected from warm surface waters, our results verify the general assumption of a biological production process as a main source of oceanic H₂ to the atmosphere rather than photochemical or other sources (Herr et al., 1981; Conrad, 1988; Punshon and Moore, 2008; Moore et al., 2009). The dominance of biological formation at higher temperatures is qualitatively consistent with the general understanding of the temperature dependence of N₂ fixation rates for N₂ fixers such as e.g. *Trichodesmium* spec., which exhibit highest N₂ fixation rates within a temperature range between 24 to 30 °C (Breitbarth et al., 2007; Stal, 2009). In fact, the saturations also show a correlation with temperature, but less clear than for δD (Fig. 7d), presumably due to simultaneous uptake and consumption processes in a complex microbial community.

However, this clear attribution is only valid in water masses with higher temperatures and the unexpectedly high δD values in cooler waters indicate the influence of other

processes. The isotopic enrichment that is expected for removal of H_2 (Chen et al., 2015; Rahn et al., 2003; Constant et al., 2015) is highly unlikely to cause a shift of almost 400‰ in δD from an assumed pure biological source, because in this case the removed fraction would have to be unrealistically large, as also recently argued for soil emitted H_2 (Chen et al., 2015). We suggest that a source of H_2 must exist in these surface waters, which produces H_2 that is out of isotope equilibrium with the water. This can be either one single source with an isotopic signature of approximately -250 ‰, or an even more isotopically enriched source that mixes with the depleted biological source.

Punshon and Moore (2008a, and references therein), reported abiotic photochemical H_2 production from CDOM and small organic compounds such as acetaldehyde or syringic acid. Walter et al. (2013) indicated, that biologically active regions such as the Banc d'Arguin at the coast of Mauritania could act as a pool of precursors such as VOCs for atmospheric H_2 with high δD values. It is thus possible that abiotic photochemical production in the surface water might be an alternative source of H_2 excess, which is not isotopically equilibrated with water, especially in regions with high radiation and biological activity, and less N_2 fixation. Given the fact that the two groups of warm and cold waters are relatively well separated and there is not a continuous mixing curve between two end members, the explanation of a single different source seems more straightforward. Isotope analyses are a powerful tool to distinguish this source from biological production. Additional measurements are needed to determine the isotopic signature of such a source and investigate to which extend photochemical production contributes to the oceanic H_2 budget in colder water masses, and also update the current models. However, with an isotopic signature of approximately -250 ‰, or an even more isotopically enriched, such a source would not significantly impact the current models.

Based on their H_2 measurements, Moore et al. (2014) suggested a substantial underestimation of oceanic N_2 fixation, especially due to high H_2 supersaturations measured in the Southern Hemisphere. By using direct measurements of N_2 fixation rates

16451

a systematic underestimation by approximately 60 % was also proposed by Großkopf et al. (2012) who suggested a global marine N_2 fixation rate of $(177 \pm 8) \text{ Tg Na}^{-1}$. In order to identify a possible significant mismatch between N_2 fixation rates and total marine H_2 production, we calculated the climatological global oceanic emissions from the GEMS database using the protocol of Pieterse et al. (2013), and an assumed mean oceanic H_2 source of 5 Tg a^{-1} as given from global budget calculations. The estimated emission rates and distributions in the Atlantic Ocean (Fig. 8) are in line with the calculations of Moore et al. (2014), who reported H_2 sea-to-air fluxes mostly in the range of $(10 \pm 5) \text{ mmol m}^{-2} \text{ a}^{-1}$ and an almost equal distribution between the hemispheres.

Westberry and Siegel (2006) estimated the global nitrogen fixation rate by *Trichodesmium* blooms by using satellite ocean color data at 42 Tg Na^{-1} and an additional 20 Tg Na^{-1} under non-bloom conditions, suggesting that *Trichodesmium* is likely the dominant organism in the global ocean new nitrogen budget. The good agreement between our measurements of H_2 concentrations and δD and the model results from the TM5 model indicate that the oceanic emissions of H_2 to the atmosphere are actually well represented in current atmospheric models (Pieterse et al., 2013 and references herein). The proposed underestimate of oceanic N_2 fixation and a possible additional H_2 release during this process seems already be incorporated in the current atmospheric budgets of H_2 . Thus, supposing that both an assumed total oceanic H_2 source of 5 Tg a^{-1} to the atmosphere and a total global nitrogen fixation rate of approximately 175 Tg N a^{-1} are correct, our calculations clearly support the suggestion of Großkopf et al. (2012) that N_2 fixers other than *Trichodesmium* have been severely underestimated in the global picture and that the oceanic release ratio of H_2 to fixed N_2 clearly needs more attention. Besides *Trichodesmium*, several other N_2 -fixing organisms are known for their potential to produce hydrogen (Wilson et al., 2010a; Falcón et al., 2002, 2004; Zehr et al., 2001; Kars et al., 2009; Barz et al., 2010), and even non- N_2 -fixing organisms might play a role (Lilley et al., 1982).

16452

4 Conclusions

Identifying sources is important to consider budgets and gain insight in production and consumption processes. Although H₂ has been assumed reasonably to be produced mainly biologically in the oceans, direct evidence was lacking. Our results verify a biological production as a main source of H₂ in oceanic surface water, especially in warmer water masses. As seen from the transects, local sources are difficult to spot due to their patchiness, this should be taken into account when planning the sampling strategy.

The unexpectedly high δD values in colder temperate water masses indicate the significant influence of processes other than biological production, and additional information e.g. by isotopic composition is needed to distinguish and verify possible sources and supersaturations of dissolved oceanic H₂. Especially the investigation of the isotopic composition of possible production pathways such as abiotic photochemical H₂ production needs further attention and should be an upcoming issue.

The pattern of mole fractions and isotopic composition of H₂ along a north–south Atlantic transect clearly depends on season and hemisphere and are consistent with previous published data and models. A possible significant underestimation of N₂ fixation as assumed by several authors could – providing a net H₂ release rate – go along with higher H₂ emissions. However, a comparison with the TM5 model and the calculation of the climatological global oceanic emissions based on GEMS database reveal that the oceanic contribution to the global H₂ budget is reasonable and in general reproduced well and therefore a proposed underestimation in the oceanic N₂ fixation seems already be corrected (from atmospheric considerations) in the current atmospheric budgets of H₂. This also indicates, with respect to the proposed source different than biological production in colder temperate water masses, that such a source would probably not significantly impact the current models.

Besides the isotopic composition of photochemically produced H₂ the composition of N₂ fixer communities and the release ratio of H₂ to N₂ fixed needs more investigation to understand the general processes and distributions of oceanic H₂ in more detail.

16453

**The Supplement related to this article is available online at
doi:10.5194/bgd-12-16431-2015-supplement.**

Acknowledgement. We are very thankful to the crew of the RV *Polarstern* and RV *L'Atalante* for their friendly and professional help and support. This study was financed by the NWO (Netherlands Organization for Scientific Research), NWO project number 816.01.001, the EU FP7 project InGOS (GA number 284274), and the BMBF (Bundesministerium für Bildung und Forschung) project SOPRAN, grant FKZ 03F0462, grant 03F0611 and grant 03F0662.

References

- Barz, M., Beimgraben, C., Staller, T., Germer, F., Opitz, F., Marquardt, C., Schwarz, C., Gutekunst, K., Vanselow, K. H., Schmitz, R., LaRoche, J., Schulz, R., and Appel, J.: Distribution analysis of hydrogenases in surface waters of marine and freshwater environments, *PloS ONE*, 5, e13846, doi:10.1371/journal.pone.0013846, 2010.
- Batenburg, A. M., Walter, S., Pieterse, G., Levin, I., Schmidt, M., Jordan, A., Hammer, S., Yver, C., and Röckmann, T.: Temporal and spatial variability of the stable isotopic composition of atmospheric molecular hydrogen: observations at six EUROHYDROS stations, *Atmos. Chem. Phys.*, 11, 6985–6999, doi:10.5194/acp-11-6985-2011, 2011.
- Bothe, H., Neuer, G., Kalbe, I., and Eisbrenner, G.: Electron donors and hydrogenase in nitrogen-fixing microorganisms, in: *Nitrogen Fixation, Annual Proceedings of the Phytochemical Society of Europe*, Nr. 18, Academic Press, London, ISBN 0-12-669450-8, 83-112, 1980.
- Bothe, H., Schmitz, O., Yates, M. G., and Newton, W. E.: Nitrogen fixation and hydrogen metabolism in cyanobacteria, *MMBR*, 74, 529–51, doi:10.1128/MMBR.00033-10, 2010.
- Breitbarth, E., Oschlies, A., and LaRoche, J.: Physiological constraints on the global distribution of *Trichodesmium* – effect of temperature on diazotrophy, *Biogeosciences*, 4, 53–61, doi:10.5194/bg-4-53-2007, 2007.
- Bottlinga, Y.: Calculated fractionation factors for carbon and hydrogen isotope exchange in the system calcite–carbon dioxide–graphite–methane–hydrogen–water vapour, *Geochim. Cosmochim. Ac.*, 33, 49–64, 1969.

16454

- Chen, Q., Popa, E. M., Batenburg, A. M., and Röckmann, T.: Isotopic signatures of production and uptake of H₂ by soil, *Atmos. Chem. Phys. Discuss.*, 15, 23457–23506, doi:10.5194/acpd-15-23457-2015, 2015.
- Conrad, R. and Seiler, W.: Methane and hydrogen in seawater (Atlantic Ocean), *Deep-Sea Res.*, 35, 1903–1917, 1988.
- Constant, P., Walter, S., Batenburg, A. M., Liot, Q., and Röckmann, T.: Kinetics and isotopic signature of the H₂ uptake activity of three Actinobacteria scavenging atmospheric H₂, in preparation, 2015.
- Ehhalt, D. H. and Rohrer, F.: The tropospheric cycle of H₂: a critical review, *Tellus B*, 61, 500–535, 2009.
- Erickson, D. J. and Taylor, J. A.: 3-D Tropospheric CO modeling: the possible influence of the ocean, *Geophys. Res. Lett.*, 19, 1955–1958, 1992.
- Falcón, L. I., Cipriano, F., Chistoserdov, A. Y., and Carpenter, E. J.: Diversity of diazotrophic unicellular cyanobacteria in the tropical North Atlantic Ocean, *Appl. Environ. Microb.*, 68, 5760–5764, doi:10.1128/AEM.68.11.5760.2002, 2002.
- Falcón, L. I., Carpenter, E. J., Cipriano, F., Bergman, B., and Capone, D. G.: N₂ fixation by unicellular bacterioplankton from the Atlantic and Pacific Oceans: phylogeny and in situ rates, *Appl. Environ. Microb.*, 70, 765–770, doi:10.1128/AEM.70.2.765-770.2004, 2004.
- Feck, T., Grooß, J.-U., and Riese, M.: Sensitivity of Arctic ozone loss to stratospheric H₂O, *Geophys. Res. Lett.*, 35, L01803, doi:10.1029/2007GL031334, 2008.
- Feilberg, K. L., Johnson, M. S., Bacak, A., Röckmann, T., and Nielsen, C. J.: Relative tropospheric photolysis rates of HCHO and HCDO measured at the European photoreactor facility, *J. Phys. Chem. A*, 111, 9034–9046, 2007.
- Gerst, S. and Quay, P.: Deuterium component of the global molecular hydrogen cycle, *J. Geophys. Res.*, 106, 5021–5031, 2001.
- Großkopf, T., Mohr, W., Baustian, T., Schunck, H., Gill, D., Kuypers, M. M. M., Lavik, G., Schmitz, R. A., Wallace, D. W. R., and LaRoche, J.: Doubling of marine dinitrogen-fixation rates based on direct measurements, *Nature*, 488, 361–364, doi:10.1038/nature11338, 2012.
- Hanschmann, T., Deneke, H., Roebeling, R., and Macke, A.: Evaluation of the shortwave cloud radiative effect over the ocean by use of ship and satellite observations, *Atmos. Chem. Phys.*, 12, 12243–12253, doi:10.5194/acp-12-12243-2012, 2012.

16455

- Hauglustaine, D. A. and Ehhalt, D. H.: A three-dimensional model of molecular hydrogen in the troposphere, *J. Geophys. Res.*, 107, 4330–4346, doi:10.1029/2001JD001156, 2002.
- Herr, F. L.: Dissolved hydrogen in Eurasian Arctic waters, *Tellus*, 36B, 55–66, 1984.
- Herr, F. L., Scranton, M. I., and Barger, W. R.: Dissolved hydrogen in the Norwegian Sea: mesoscale surface variability and deep-water distribution, *Deep-Sea Res.*, 28A, 1001–1016, 1981.
- Herr, F. L., Frank, E. C., Leone, G. M., and Kennicutt, M. C.: Diurnal variability of dissolved molecular hydrogen in the tropical South Atlantic Ocean, *Deep-Sea Res.*, 31, 13–20, 1984.
- Houweling, S., Dentener, F., and Lelieveld, J.: The impact of non-methane hydrocarbon compounds on tropospheric photochemistry, *J. Geophys. Res.*, 103, 10673–10696, doi:10.1029/97JD03582, 1998.
- Jacobson, M. Z.: Effects of wind-powered hydrogen fuel cell vehicles on stratospheric ozone and global climate, *Geophys. Res. Lett.*, 35, L19803, doi:10.1029/2008GL035102, 2008.
- Jacobson, M. Z., Colella, W. G., and Golden, D. M.: Cleaning the air and improving health with hydrogen fuel-cell vehicles, *Science*, 308, 1901–1905, 2005.
- Jordan, A. and Steinberg, B.: Calibration of atmospheric hydrogen measurements, *Atmos. Meas. Tech.*, 4, 509–521, doi:10.5194/amt-4-509-2011, 2011.
- Kars, G., Gündüz, U., Yücel, M., Rakhely, G., Kovacs, K. L., and Eroğlu, I.: Evaluation of hydrogen production by *Rhodobacter sphaeroides* O. U.001 and its hupSL deficient mutant using acetate and malate as carbon sources, *Int. J. Hydrogen. Energ.*, 34, 2184–2190, doi:10.1016/j.ijhydene.2009.01.016, 2009.
- Knox, M., Quay, P. D., and Wilbur, D.: Kinetic isotopic fractionation during air–water gas transfer of O₂, N₂, CH₄, and H₂, *J. Geophys. Res.*, 97, 20335–20343, 1992.
- Kock, A., Gebhardt, S., and Bange, H. W.: Methane emissions from the upwelling area off Mauritania (NW Africa), *Biogeosciences*, 5, 1119–1125, doi:10.5194/bg-5-1119-2008, 2008.
- Krol, M., Houweling, S., Bregman, B., van den Broek, M., Segers, A., van Velthoven, P., Peters, W., Dentener, F., and Bergamaschi, P.: The two-way nested global chemistry-transport zoom model TM5: algorithm and applications, *Atmos. Chem. Phys.*, 5, 417–432, doi:10.5194/acp-5-417-2005, 2005.
- Lilley, M. D., Baross, J. A., and Gordon, L. I.: Dissolved hydrogen and methane in Saanieh Inlet, British Columbia, *Deep-Sea Res.*, 29, 1471–1484, doi:10.1016/0198-0149(82)121471-13, 1982.
- Longhurst, A. R.: *Ecological Geography of the Sea*, Academic, San Diego, California, 398 pp., 1998.

16456

- Moore, R. M., Punshon, S., Mahaffey, C., and Karl, D.: The relationship between dissolved hydrogen and nitrogen fixation in ocean waters, *Deep-Sea Res.*, 56, 1449–1458, doi:10.1016/j.dsr.2009.04.008, 2009.
- Moore, R. M., Kienast, M., Fraser, M., Cullen, J. J., Deutsch, C., Dutkiewicz, S., Follows, M. J., and Somes, C. J.: Extensive hydrogen supersaturations in the western South Atlantic Ocean suggest substantial underestimation of nitrogen fixation, *J. Geophys. Res.-Oceans*, 119, 4340–4350, doi:10.1002/2014JC010017, 2014.
- Nilsson, E. J. K., Johnson, M. S., Taketani, F., Matsumi, Y., Hurley, M. D., and Wallington, T. J.: Atmospheric deuterium fractionation: HCHO and HCDO yields in the $\text{CH}_2\text{DO} + \text{O}_2$ reaction, *Atmos. Chem. Phys.*, 7, 5873–5881, doi:10.5194/acp-7-5873-2007, 2007.
- Nilsson, E. J. K., Andersen, V. F., Skov, H., and Johnson, M. S.: Pressure dependence of the deuterium isotope effect in the photolysis of formaldehyde by ultraviolet light, *Atmos. Chem. Phys.*, 10, 3455–3462, doi:10.5194/acp-10-3455-2010, 2010.
- Novelli, P. C., Lang, P. M., Masarie, K. A., Hurst, D. F., Myers, R., and Elkins, J. W.: Molecular hydrogen in the troposphere: global distribution and budget, *J. Geophys. Res.*, 104, 30427–30444, 1999.
- Pieterse, G., Krol, M. C., and Röckmann, T.: A consistent molecular hydrogen isotope chemistry scheme based on an independent bond approximation, *Atmos. Chem. Phys.*, 9, 8503–8529, doi:10.5194/acp-9-8503-2009, 2009.
- Pieterse, G., Krol, M. C., Batenburg, A. M., Steele, L. P., Krummel, P. B., Langenfelds, R. L., and Röckmann, T.: Global modelling of H_2 mixing ratios and isotopic compositions with the TM5 model, *Atmos. Chem. Phys.*, 11, 7001–7026, doi:10.5194/acp-11-7001-2011, 2011.
- Pieterse, G., Krol, M. C., Batenburg, A. M., Brenninkmeijer, C. A. M., Popa, M. E., O'Doherty, S., Grant, A., Steele, L. P., Krummel, P. B., Langenfelds, R. L., Wang, H. J., Vermeulen, A. T., Schmidt, M., Yver, C., Jordan, A., Engel, A., Fisher, R. E., Lowry, D., Nisbet, E. G., Reimann, S., Vollmer, M. K., Steinbacher, M., Hammer, S., Forster, G., Sturges, W. T., and Röckmann, T.: Reassessing the variability in atmospheric H_2 using the two-way nested TM5 model, *J. Geophys. Res.-Atmos.*, 118, 3764–3780, doi:10.1002/jgrd.50204, 2013.
- Popa, M. E., Vollmer, M. K., Jordan, A., Brand, W. A., Pathirana, S. L., Rothe, M., and Röckmann, T.: Vehicle emissions of greenhouse gases and related tracers from a tunnel study: $\text{CO} : \text{CO}_2$, $\text{N}_2\text{O} : \text{CO}_2$, $\text{CH}_4 : \text{CO}_2$, $\text{O}_2 : \text{CO}_2$ ratios, and the stable isotopes ^{13}C and ^{18}O in CO_2 and CO , *Atmos. Chem. Phys.*, 14, 2105–2123, doi:10.5194/acp-14-2105-2014, 2014.

16457

- Popa, M. E., Segers, A. J., van der Gon, H. A. C. D., Krol, M. C., Visschedijk, A. J. H., Schaap, M., and Röckmann, T.: Impact of a future H_2 transportation on atmospheric pollution in Europe, *Atmos. Environ.*, 113, 208–222, doi:10.1016/j.atmosenv.2015.03.022, 2015.
- Prather, M. J.: An environmental experiment with H_2 ?, *Science*, 302, 581–582, 2003.
- Price, H., Jaegle, L., Rice, A., Quay, P., Novelli, P. C., Gammon, R.: Global budget of molecular hydrogen and its deuterium content: constraints from ground station, cruise, and aircraft observations, *J. Geophys. Res.*, 112, D22108, doi:10.1029/2006JD008152, 2007.
- Punshon, S., Moore, R. M., and Xie, H.: Net loss rates and distribution of molecular hydrogen (H_2) in mid-latitude coastal waters, *Mar. Chem.*, 105, 129–139, doi:10.1016/j.marchem.2007.01.009, 2007.
- Punshon, S. and Moore, R.: Photochemical production of molecular hydrogen in lake water and coastal seawater, *Mar. Chem.*, 108, 215–220, doi:10.1016/j.marchem.2007.11.010, 2008a.
- Punshon, S. and Moore, R. M.: Aerobic hydrogen production and dinitrogen fixation in the marine cyanobacterium *Trichodesmium erythraeum* IMS101, *Limnol. Oceanogr.*, 53, 2749–2753, 2008b.
- Rahn, T., Kitchen, N., and Eiler, J. M.: D/H ratios of atmospheric H_2 in urban air: results using new methods for analysis of nano-molar H_2 samples, *Geochim. Cosmochim. Ac.*, 66, 2475–2481, 2002.
- Rahn, T., Eiler, J. M., Boering, K. A., Wennberg, P. O., McCarthy, M. C., Tyler, S., Schauffler, S., Donnelly, S., and Atlas, E.: Extreme deuterium enrichment in stratospheric hydrogen and the global atmospheric budget of H_2 , *Nature*, 424, 918–921, 2003.
- Rhee, T. S., Mak, J., Röckmann, T., and Brenninkmeijer, C. A. M.: Continuous-flow isotope analysis of the deuterium/hydrogen ratio in atmospheric hydrogen, *Rapid Commun. Mass. Sp.*, 18, 299–306, doi:10.1002/rcm.1309, 2004.
- Rhee, T. S., Brenninkmeijer, C. A. M., and Röckmann, T.: The overwhelming role of soils in the global atmospheric hydrogen cycle, *Atmos. Chem. Phys.*, 6, 1611–1625, doi:10.5194/acp-6-1611-2006, 2006.
- Rice, A., Quay, P., Stutsman, J., Gammon, R., Price, H., and Jaegle, L.: Meridional distribution of molecular hydrogen and its deuterium content in the atmosphere, *J. Geophys. Res.*, 115, D12306, doi:10.1029/2009JD012529, 2010.
- Robinson, C., Holligan, P., Jickels, T., and Lavender, S.: The Atlantic Meridional Transect Programme (1995–2012), *Deep-Sea Res. Pt. II*, 56, 895–898, doi:10.1016/j.dsr.2008.10.005, 2009.

16458

- Röckmann, T., Rhee, T. S., and Engel, A.: Heavy hydrogen in the stratosphere, *Atmos. Chem. Phys.*, 3, 2015–2023, doi:10.5194/acp-3-2015-2003, 2003.
- Röckmann, T., Gómez Álvarez, C. X., Walter, S., van Veen, C., Wollny, A. G., Gunthe, S. S., Helas, G., Pöschl, U., Keppler, F., Greule, M., and Brand, W. A.: The isotopic composition of H₂ from wood burning – dependency on combustion efficiency, moisture content and δD of local precipitation, *J. Geophys. Res.*, 115, D17308, doi:10.1029/2009JD013188, 2010a.
- Röckmann, T., Walter, S., Bohn, B., Wegener, R., Spahn, H., Brauers, T., Tillmann, R., Schlosser, E., Koppmann, R., and Rohrer, F.: Isotope effect in the formation of H₂ from H₂CO studied at the atmospheric simulation chamber SAPHIR, *Atmos. Chem. Phys.*, 10, 5343–5357, doi:10.5194/acp-10-5343-2010, 2010b.
- Schlitzer, R.: Ocean Data View 4, available at: <http://odv.awi.de> (last access: 5 October 2015), 2012.
- Schultz, M. G., Diehl, T., Basseur, G. P., and Zittel, W.: Air pollution and climate–forcing impacts of a global hydrogen economy, *Science*, 302, 624–627, 2003.
- Schütz, K., Happe, T., Troshina, O., Lindblad, P., Leitão, E., Oliveira, P., and Tamagnini, P.: Cyanobacterial H₂ production – a comparative analysis, *Planta*, 218, 350–359, doi:10.1007/s00425-003-1113-5, 2004.
- Scranton, M., Jones, M., and Herr, F. L.: Distribution and variability of hydrogen in the Mediterranean Sea, *J. Mar. Res.*, 40, 873–891, 1982.
- Scranton, M. I.: The role of the cyanobacterium *Oscillatoria (Trichodesmium) thiebautii* in the marine hydrogen cycle, *Mar. Ecol.*, 11, 79–87, 1983.
- Seiler, W. and Schmidt, U.: Dissolved non–conservative gases in seawater, in: *The Sea*, Vol 5., edited by: Goldberg E. D., John Wiley & Sons, New York, 219–243, 1974.
- Stal, L. J.: Is the distribution of nitrogen-fixing cyanobacteria in the oceans related to temperature?, *Environ. Microbiol.*, 11, 1632–1645, doi:10.1111/j.1758-2229.2009.00016.x, 2009.
- Tamagnini, P., Leitão, E., Oliveira, P., Ferreira, D., Pinto, F., Harris, D. J., Heidorn, T., and Lindblad, P.: Cyanobacterial hydrogenases: diversity, regulation and applications, *FEMS Microbiol. Rev.*, 31, 692–720, doi:10.1111/j.1574-6976.2007.00085.x, 2007.
- Tromp, T. K., Shia, R.-L., Allen, M., Eiler, J. M., and Yung, Y. L.: Potential environmental impact of a hydrogen economy on the stratosphere, *Science*, 300, 1740–1742, 2003.
- Vollmer, M. K., Walter, S., Bond, S. W., Soltic, P., and Röckmann, T.: Molecular hydrogen (H₂) emissions and their isotopic signatures (H/D) from a motor vehicle: implications on atmospheric H₂, *Atmos. Chem. Phys.*, 10, 5707–5718, doi:10.5194/acp-10-5707-2010, 2010.

16459

- Vollmer, M. K., Jordan, A., Brand, W. A., Pathirana, S. L., Rothe, M., and Röckmann, T.: Vehicle emissions of greenhouse gases and related tracers from a tunnel study: CO: CO₂, N₂O: CO₂, CH₄: CO₂, O₂: CO₂ ratios, and the stable isotopes ¹³C and ¹⁸O in CO₂ and CO, *Atmos. Chem. Phys.*, 14, 2105–2123, doi:10.5194/acp-14-2105-2014, 2014.
- Walter, S., Laukenmann, S., Stams, A. J. M., Vollmer, M. K., Gleixner, G., and Röckmann, T.: The stable isotopic signature of biologically produced molecular hydrogen (H₂), *Biogeosciences* 9, 4115–4123, doi:10.5194/bg-9-4115-2012, 2012.
- Walter, S., Kock, A., and Röckmann, T.: High-resolution measurements of atmospheric molecular hydrogen and its isotopic composition at the West African coast of Mauritania, *Biogeosciences*, 10, 3391–3403, doi:10.5194/bg-10-3391-2013, 2013.
- Warwick, N. J., Bekki, S., Nisbet, E. G., and Pyle, J. A.: Impact of a hydrogen economy on the stratosphere and troposphere studied in a 2-D model, *Geophys. Res. Lett.*, 31, L05107, doi:10.1029/2003GL019224, 2004.
- Westberry, T. K. and Siegel, D. A.: Spatial and temporal distribution of *Trichodesmium* blooms in the world's oceans, *Global Biogeochem. Cy.*, 20, GB4016, doi:10.1029/2005GB002673, 2006.
- Wiesenburg, D. A. and Guinasso, N. L.: Equilibrium solubilities of methane, carbon monoxide, and hydrogen in water and sea water, *J. Chem. Eng. Data*, 24, 356–360, doi:10.1021/je60083a006, 1979.
- Wilson, S. T., Foster, R. A., Zehr, J. P., and Karl, D. M.: Hydrogen production by *Trichodesmium erythraeum*, *Cyanothece* sp., and *Crocospaera watsonii*, *Aquat. Microb. Ecol.*, 59, 197–206, doi:10.3354/ame01407, 2010a.
- Wilson, S. T., Tozzi, S., Foster, R. A., Ilikchyan, I., Kolber, Z. S., Zehr, J. P., and Karl, D. M.: Hydrogen cycling by the unicellular marine diazotrophs *Crocospaera watsonii* strain WH8501, *Appl. Environ. Microb.*, 76, 6797–803, doi:10.1128/AEM.01202-10, 2010b.
- Wilson, S. T., del Valle, D. A., Robidart, J. C., Zehr, J. P., and Karl, D. M.: Dissolved hydrogen and nitrogen fixation in the oligotrophic North Pacific Subtropical Gyre, *Environ. Microbiol. Rep.*, 5, 697–704, doi:10.1111/1758-2229.12069, 2013.
- Yashiro, H., Sudo, K., Yonemura, S., and Takigawa, M.: The impact of soil uptake on the global distribution of molecular hydrogen: chemical transport model simulation, *Atmos. Chem. Phys.*, 11, 6701–6719, doi:10.5194/acp-11-6701-2011, 2011.

16460

- Yonemura, S., Kawashima, S., and Tsuruta, H.: Carbon monoxide, hydrogen, and methane uptake by soils in a temperate arable field and a forest, *J. Geophys. Res.*, 105, 14347–14362, doi:10.1029/1999JD901156, 2000.
- Yver, C. E., Pison, I. C., Fortems-Cheiney, A., Schmidt, M., Chevallier, F., Ramonet, M., Jordan, A., Søvdé, O. A., Engel, A., Fisher, R. E., Lowry, D., Nisbet, E. G., Levin, I., Hammer, S., Necki, J., Bartyzel, J., Reimann, S., Vollmer, M. K., Steinbacher, M., Aalto, T., Maione, M., Arduini, J., O'Doherty, S., Grant, A., Sturges, W. T., Forster, G. L., Lunder, C. R., Privalov, V., Paramonova, N., Werner, A., and Bousquet, P.: A new estimation of the recent tropospheric molecular hydrogen budget using atmospheric observations and variational inversion, *Atmos. Chem. Phys.*, 11, 3375–3392, doi:10.5194/acp-11-3375-2011, 2011.
- Zehr, J. P., Waterbury, J. B., Turner, P. J., Montoya, J. P., Omoregie, E., Steward, G. F., Hansen, A., and Karl, D. M.: Unicellular cyanobacteria fix N₂ in the subtropical North Pacific Ocean, *Nature*, 412, 635–638, 2001.

16461

Table 1. Overview of sample distribution during the cruises: type A are discrete atmospheric samples, type H are headspace samples extracted from the surface water. The sample numbers in brackets give the number of measured samples in the northern (NH) and southern (SH) hemisphere.

Cruise	Date	Position (start–end)	Nr. of Samples (NH/SH)	Type
ANT-XXIV/4	18 Apr–20 May 2008	59.15° W/46.13° S – 06.21° W/47.96° N	95 (44 NH/51 SH)	A
ANT-XXV/5	11 Apr–24 May 2009	50.99° W/40.82° S – 23.05° W/16.55° N	91 (30 NH/61 SH)	A
ANT XXVI/1	16 Oct–25 Nov 2009	12.05° W/37.96° N – 47.28° W/37.43° S	60 (29 NH/31 SH)	A
ANT XXVI/4	07 Apr–17 May 2010	58.14° W/43.75° S – 04.46° E/53.15° N	114 (56 NH/58 SH)	A
ANT XXVI/4	07 Apr–17 May 2010	32.53° W/18.79° S – 13.00° W/36.54° N	16 (10 NH/6 SH)	H
L'Atalante ATA-3	03 Feb–20 Feb 2008	17.83° N/16.56° W – 17.60° N/24.24° W	6 (6 NH/0 SH)	H

16462

Table 2. Hemispheric means of atmospheric H₂ and its isotopic composition along the four meridional Atlantic transects.

Cruise	Southern Hemisphere				Northern Hemisphere				
	IRMS – H ₂ mole fraction [ppb]	δD [‰]	RGA – H ₂ mole fraction [ppb]	RGA – CO mole fraction [ppb]	IRMS – H ₂ mole fraction [ppb]	δD [‰]	RGA – H ₂ mole fraction [ppb]	RGA – CO mole fraction [ppb]	
ANT-XXI/4 Apr 2008	mean range <i>n</i>	543.4 ± 7.3 528.8–568.5 49 (2 values excluded)	145.4 ± 5.3 135.4–155.7 49 (2 values excluded)	No data No data	544.1 ± 9.8 522.0–567.8 44	118.6 ± 3.9 110.4–130.9 44	No data	No data	
ANT-XXV/5 Apr 2009	mean range <i>n</i>	533.9 ± 38.7 350.2–631.9 60	140.5 ± 21.1 20.9–166.1 60	520.4 ± 24.0 432.5–545.1 21	59.9 ± 17.7 43.6–119.6 21	532.94 ± 19.73 466.9–560.3 28 (2 values excluded)	121.28 ± 7.09 89.1–130.9 28 (2 values excluded)	526.18 ± 12.6 508.9–564.1 29	112.67 ± 21.3 76.9–190.5 29
ANT XXVI/1 Oct 2009	mean range <i>n</i>	548.5 ± 6.8 535.9–563.4 30 (1 value excluded)	143.2 ± 4.2 135.5–149.3 30 (1 value excluded)	546.4 ± 7.4 531.4–563.0 49	59.9 ± 10.5 47.7–85.8 49	532.04 ± 10.65 501.1–551.7 29	133.94 ± 4.43 123.5–141.7 29	526.02 ± 10.53 494.2–548.8 46	76.73 ± 7.43 65.4–96.1 46
ANT XXVI/4 Apr 2010	mean range <i>n</i>	541.6 ± 16.3 496.0–579.6 58	143.7 ± 11.5 89.3–161.8 58	525.1 ± 29.1 481.5–696.8 617	47.2 ± 8.8 36.2–121.8 617	539.4 ± 14.8 505.5–564.6 56	116.2 ± 11.5 93.8–146.6 56	507.8 ± 15.7 481.3–603.8 1339	120.8 ± 11.2 72.7–146.1 1339

16463

Table 3. Overview of means of atmospheric H₂ and its isotopic composition along the five high-resolution transects of ANT-XXV/5, including the standard deviation and the range.

Transect (latitude)		Mole fraction [ppb]	δD [‰]
40.8° S/38.9° S	mean	515.5 ± 37.7	141.4 ± 6.2
<i>n</i> = 12	range	448.4–566.9	129.3–151.0
33.0° S/30.8° S	mean	521.4 ± 53.3	152.9 ± 5.9
<i>n</i> = 12	range	350.2–551.9	142.8–166.1
23.5° S/15.7° S	mean	536.9 ± 38.4	144.1 ± 41.4
<i>n</i> = 32	range	392.9–631.9	20.91–322.45
2.0° S/3.2° N	mean	537.5 ± 36.2	119.5 ± 12.6
<i>n</i> = 11	range	466.9–592.2	89.1–135.5
9.9° N/16.2° N	mean	537.0 ± 12.2	122.5 ± 3.0
<i>n</i> = 21	range	511.0–560.3	118.4–131.0

16464

Table 4. Overview of headspace sample results from the ANT-XXVI/4 cruise (2010) and the L'Atalante ATA-3 (2008): χ_h is the measured mole fraction of the headspace in parts per billion (ppb = nmole mole⁻¹), χ_a is the corresponding atmospheric mole fraction in ppb, D_h and D_a is the measured isotopic composition in permil [‰]. The H_2 equilibrium concentration c_{sat} (H_2) was determined by using the equations from Wiesenburg and Guinasso (1979), the initial dissolved H_2 concentration c_{w0} is calculated as given in the Supplement, and the excess ΔH_2 is the difference between them. δ_{w0SC1} and δ_{w0SC2} show the two scenarios to derive the initial isotope delta of dissolved H_2 . $S_{(H_2)}$ is the supersaturation of H_2 in the surface water. The calculated extraction efficiency was 92 %. The calculations are given in the Supplement in more detail.

Date/Time [UTC]	Sampling position	χ_a [ppb]	δD_a [‰]	χ_m [ppb]	δD_m [‰]	c_{sat} (H_2) [nmolL ⁻¹]	c_{w0} [nmolL ⁻¹]	Δ (H_2) [nmolL ⁻¹]	δ_{w0SC1} [‰]	δ_{w0SC2} [‰]	$S_{(H_2)}$
21 Apr 2010	-18.79° N	562.0	148.5	653.3	-37.3	0.35	1.68	1.32	-536.2	-535.6	3.75
15:15	-32.53° E										
22 Apr 2010	-15.91° N	524.2	134.5	750.6	-138.6	0.33	2.89	2.57	-654.8	-654.4	7.80
15:24	-30.49° E										
23 Apr 2010	-13.06° N	551.6	144.3	754.4	-125.1	0.35	2.91	3.57	-602.9	-602.5	7.41
15:21	-28.51° E										
24 Apr 2010	-10.71° N	522.0	153.2	797.0	-151.2	0.33	3.52	3.19	-605.6	-605.2	9.74
15:36	-26.92° E										
25 Apr 2010	-7.97° N	542.9	154.7	674.8	-59.4	0.34	1.97	1.63	-566.1	-565.6	4.81
15:24	-26.02° E										
26 Apr 2010	-5.16° N	517.8	149.7	584.5	9.2	0.32	0.83	0.51	-654.0	-653.6	1.56
15:12	-23.11° E										
28 Apr 2010	1.78° N	540.9	144.4	619.8	-33.1	0.34	1.27	0.93	-682.1	-681.8	2.76
13:54	-23.00° E										
29 Apr 2010	4.99° N	562.8	114.2	615.9	-11.7	0.35	1.25	0.89	-575.4	-574.9	2.53
14:21	-23.00° E										
30 Apr 2010	8.07° N	550.6	118.6	591.1	-0.6	0.35	0.94	0.60	-680.8	-680.5	1.71
14:15	-23.00° E										
02 May 2010	14.55° N	541.3	110.5	603.3	-15.0	0.35	1.13	0.78	-680.7	-680.4	2.24
14:39	-23.68° E										
04 May 2010	17.61° N	523.2	121.5	686.5	-83.6	0.34	2.27	1.93	-630.8	-630.3	5.74
13:39	-24.75° E										
05 May 2010	20.28° N	559.0	125.7	667.9	-55.3	0.36	2.05	1.69	-572.6	-572.2	4.66
13:21	-22.86° E										

16465

Date/Time [UTC]	Sampling position	χ_a [ppb]	δD_a [‰]	χ_m [ppb]	δD_m [‰]	c_{sat} (H_2) [nmolL ⁻¹]	c_{w0} [nmolL ⁻¹]	Δ (H_2) [nmolL ⁻¹]	δ_{w0SC1} [‰]	δ_{w0SC2} [‰]	$S_{(H_2)}$
06 May 2010	23.12° N	550.7	104.3	586.6	-1.1	0.36	0.93	0.57	-719.3	-719.0	1.58
12:30	-20.66° E										
07 May 2010	25.07° N	539.8	108.9	575.3	20.3	0.35	0.79	0.43	-645.2	-644.8	1.21
12:18	-17.50° E										
09 May 2010	33.60° N	546.8	104.6	624.2	21.0	0.37	1.51	1.14	-327.2	-326.4	3.10
12:51	-13.86° E										
10 May 2010	36.53° N	531.8	107.8	571.6	62.0	0.36	0.77	0.41	-230.2	-229.3	1.13
12:55	-13.01° E										
09 Feb 2008	16.91° N	527.2	118.4	141.7	-224.09	0.35	1.57	1.22	-221.8	-221.0	3.46
16:05	-16.82° E										
11 Feb 2008	18.77° N	538.5	115.3	550.4	-383.39	0.36	5.91	5.54	-381.6	-380.9	15.28
17:58	-16.81° E										
15 Feb 2008	17.93° N	536.8	112.2	138.8	-114.85	0.36	1.79	1.42	-112.2	-111.3	3.92
10:27	-16.38° E										
16 Feb 2008	17.72° N	548.4	120.0	20.3	-180.51	0.37	0.50	0.13	-179.0	-178.2	0.35
6:05	-16.60° E										
16 Feb 2008	18.01° N	548.4	120.0	31.0	-218.73	0.37	0.72	0.35	-217.3	-216.5	0.94
17:41	-17.01° E										
18 Feb 2008	18.00° N	541.8	126.5	48.9	-321.61	0.36	1.16	0.80	-320.4	-319.7	2.22
18:22	-23.00° E										

16466

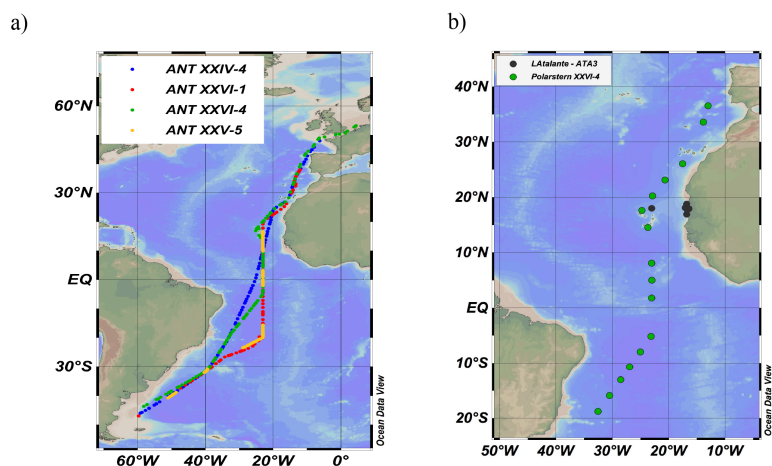


Figure 1. (a) Cruise tracks of the RV Polarstern, dots indicate positions of discrete atmospheric air sampling, (b) positions of surface water headspace sampling during ANT-XXVI/4 ($n = 16$, green dots) and the RV L'Atalante ATA-3 cruise ($n = 6$, black dots).

16467

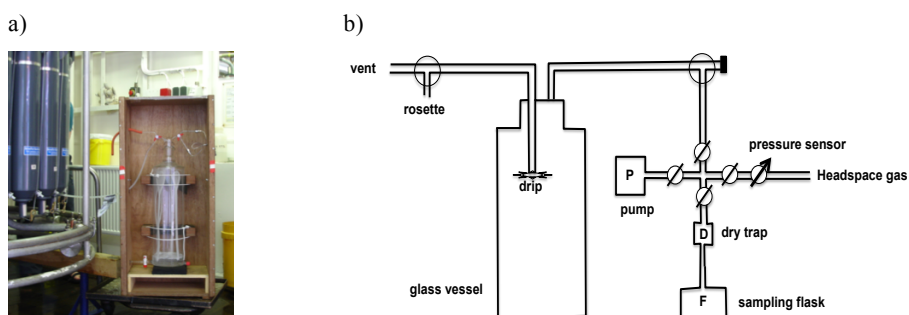


Figure 2. Experimental setup for headspace sampling, (a) sampling of the surface water into the glass vessel, connected to the Niskin bottle rosette, (b) scheme of the experimental setup.

16468

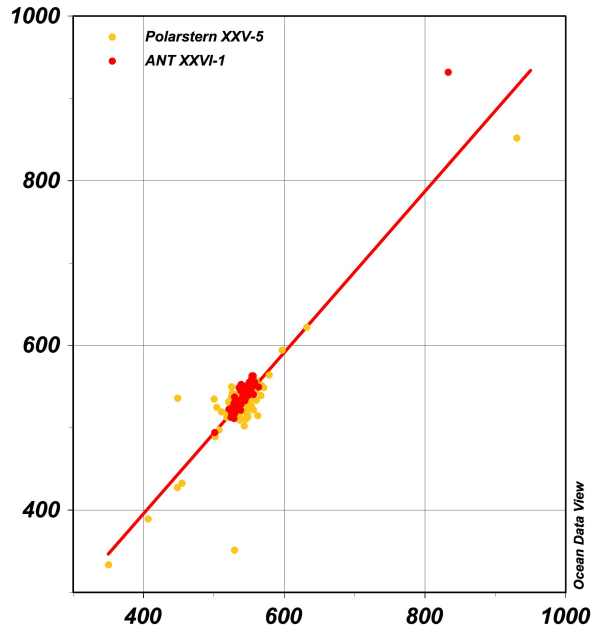
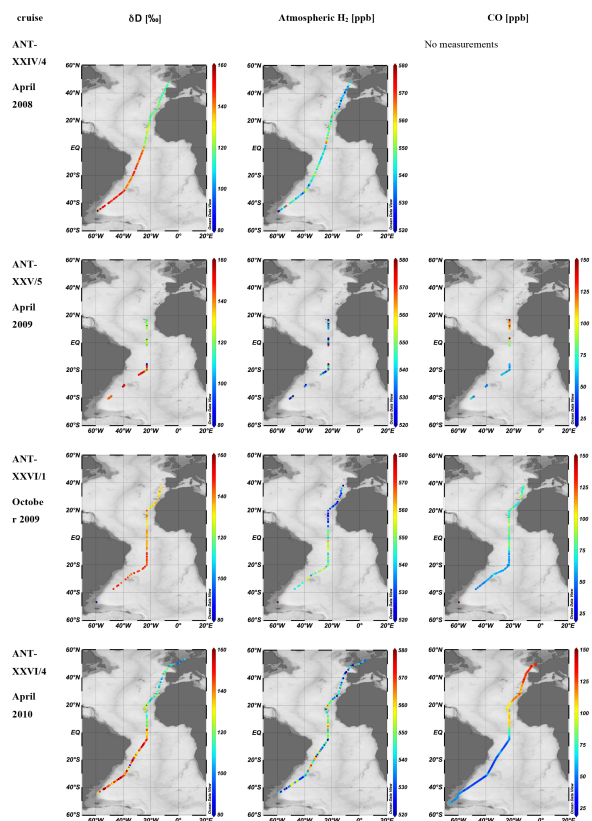


Figure 3. Comparing the H₂ mole fractions [ppb] measured with the isotopic experimental setup (*x* axis) and the Peak Performer 1 RGA (*y* axis) during ANT-XXVI/1 (red labeled) and ANT-XXV/5 (yellow labeled), $y = 0.979x + 3.96$, $R^2 = 0.81$, $n = 147$.

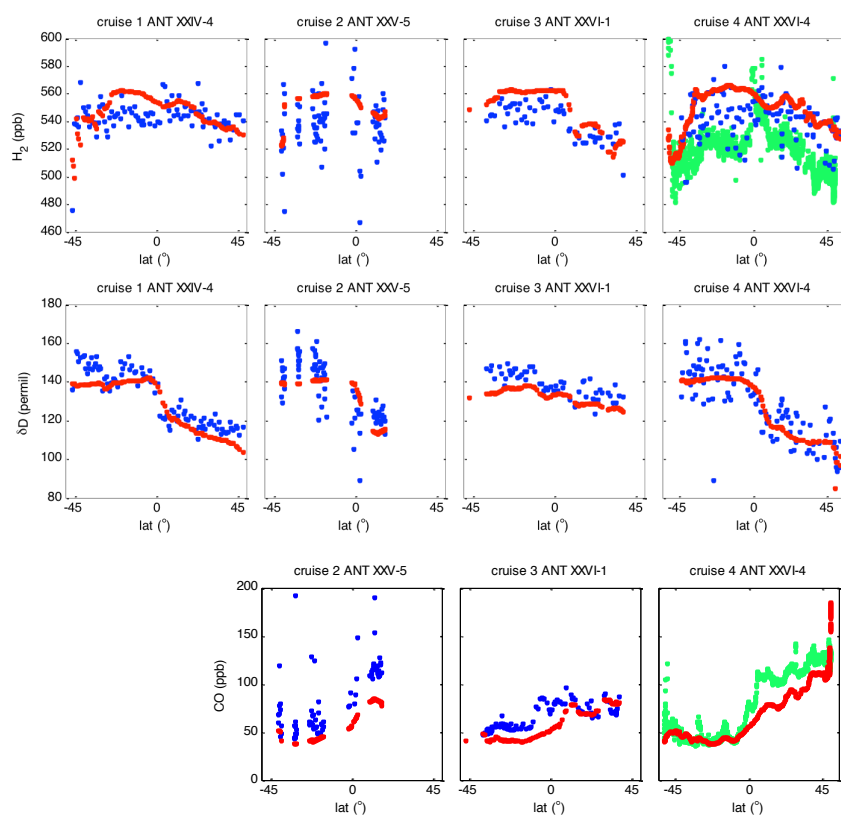
16469



16470

Figure 4. δD (H_2) [‰] (first column), H_2 mole fraction [ppb] (second column), and CO mole fraction [ppb] (third column), along the meridional cruise tracks of RV Polarstern, the mole fraction and δD of H_2 are measured by IRMS, the CO mole fraction by RGA.

16471



16472

Figure 5. Comparison of measurement results of H₂ and CO mole fractions and δD with TM5 model results (given in red). Data are shown against latitude. The blue markers show results of flask samples, the green markers represent the continuous in-situ measurements (performed with the peak performer instrument on-board). CO has not been analysed in the flasks sampled during the last cruise. The model data were interpolated at the place and time of sampling or measurements.

16473

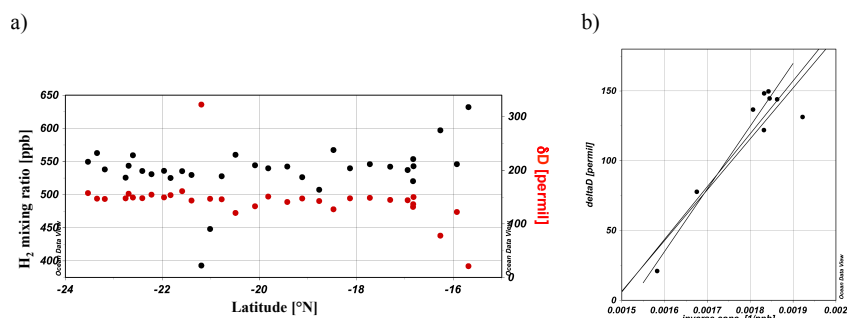
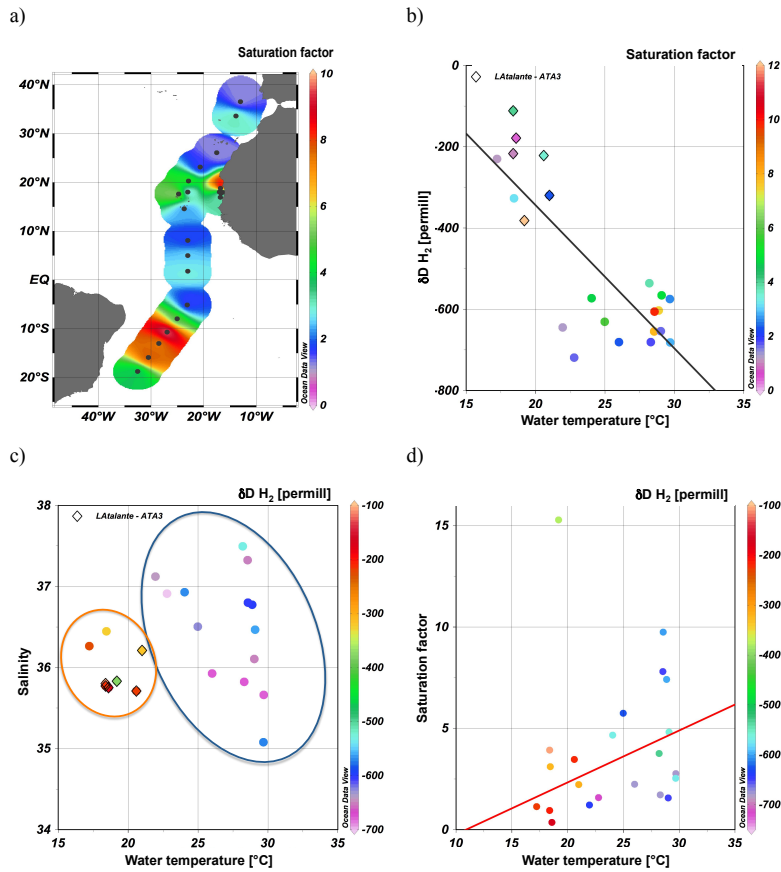


Figure 6. (a) H₂ mole fraction [ppb] (black) and δD [‰] (red) along the ANT-XXV/5 high-resolution transect 24–15° S, **(b)** keeling plot of the samples along the high-resolution transect north of 18° S. The three trend lines indicate the range of the Keeling plot analysis that was applied to determine the source signature.

16474



16475

Figure 7. (a) H₂ supersaturation factor in the surface water (color coded) along the RV *Polarstern* cruise track of ANT-XXVI/4 and the RV *L'Atalante* cruise ATA-3, with maxima around the Cape Verde islands and 10–15° S, note: each sample is represented by a single dot, (b) comparing the δD (H₂) at different water temperatures, the respective saturation factors are color coded, sample dots marked with a diamond belong to the RV *L'Atalante* cruise, sample dots without to the ANT-XXVI/4 cruise; $y = -35.2x + 360.9$, $R^2 = 0.66$, $n = 22$, (c) distribution of δD (H₂) (color coded) in correlation between water temperature and salinity, (d) correlation between water and saturation factor, the δD is color-coded, the exceptional high saturation above 15 has been excluded from the correlation calculation, $y = 0.26x - 2.79$, $R^2 = 0.22$, $n = 21$.

16476

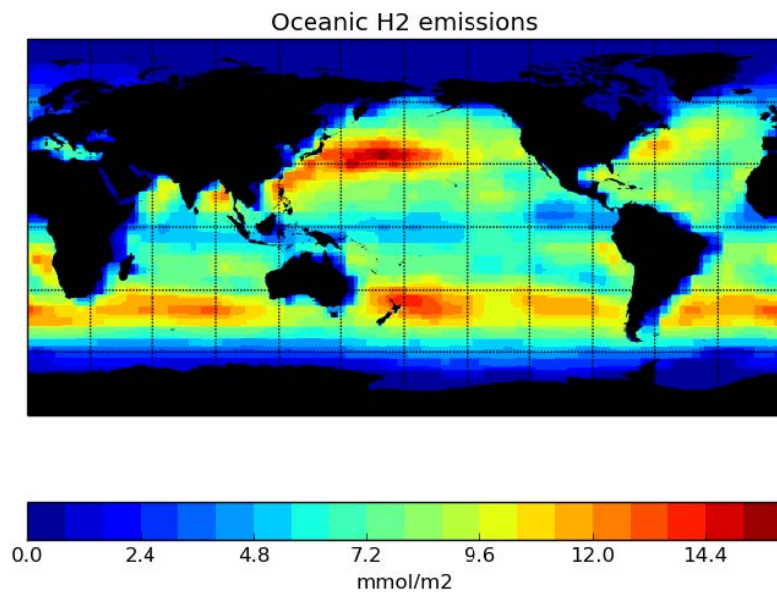


Figure 8. Oceanic H₂ emissions used in the TM5 model simulations ($\text{mmol m}^{-2} \text{a}^{-1}$, based on the distribution provided by the project GEMS (Global and regional Earth-system (Atmosphere) Monitoring using Satellite and in-situ data) and scaled to a total oceanic source of 5 Tg a^{-1} (Pieterse et al., 2013).